

Electronic Structure of Cobalt-Corrole-Pyridine Complexes: Noninnocent Five-coordinate Co(II) Corrole-Radical States

Sumit Ganguly,^a Jeanet Conradie,^b Jesper Bendix,^c Kevin J. Gagnon,^d Laura J. McCormick,^d and
Abhik Ghosh^{*,a}

^aDepartment of Chemistry, UiT – The Arctic University of Norway,
N-9037 Tromsø, Norway;

^bDepartment of Chemistry, University of the Free State, 9300 Bloemfontein,
Republic of South Africa;

^cDepartment of Chemistry, University of Copenhagen, Universitetsparken 5,
DK-2100 Copenhagen, Denmark;

^dAdvanced Light Source, Lawrence Berkeley National Laboratory,
Berkeley, CA 94720-8229, USA.

Email: abhik.ghosh@uit.no (AG)

Note! The crystal structures described in this paper have been deposited at the Cambridge Crystallographic Data Centre and assigned the deposition numbers CCDC 1565763-1565764.

Abstract. Two sets of complexes of Co-triarylcorrole-bispyridine complexes, $\text{Co}[\text{TpXPC}](\text{py})_2$ and $\text{Co}[\text{Br}_8\text{TpXPC}](\text{py})_2$ have been synthesized, where TpXPC refers to a *meso*-tris(*para*-X-phenyl)corrole ligand with $X = \text{CF}_3, \text{H}, \text{Me},$ and OMe and Br_8TpXPC to the corresponding β -octabrominated ligand. The axial pyridines in these complexes were found to be labile and, in dilute solutions in dichloromethane, the complexes dissociate almost completely to the five-coordinate monopyridine complexes. Upon addition of a small quantity of pyridine, the complexes revert back to the six-coordinate forms. These transformations are accompanied by dramatic changes in color and optical spectra. ^1H NMR spectroscopy and X-ray crystallography have confirmed that the bispyridine complexes are authentic low-spin Co(III) species. Strong substituent effects on the Soret maxima and broken-symmetry DFT calculations, on the other hand, indicate a Co^{II} -corrole $^{2-}$ formulation for the five-coordinate $\text{Co}[\text{TpXPC}](\text{py})$ series. The calculations implicate a $\text{Co}(d_{z^2})$ -corrole(a_{2u}) orbital interaction as responsible for the metal-ligand antiferromagnetic coupling that leads to the open-shell singlet ground state of these species. Furthermore, the calculations predict two low-energy $S = 1$ intermediate-spin Co(III) states, a scenario that we have been able to experimentally corroborate with temperature-dependent EPR studies. Our findings add to the growing body of evidence for noninnocent electronic structures among first-row transition metal corrole derivatives.

Introduction. Cobalt-corrole-bispyridine complexes, $\text{Co}[\text{Cor}](\text{py})_2$, are currently of great interest as efficient catalysts of both proton reduction and water oxidation under ambient conditions.^{1,2,3,4,5} An essential aspect of the catalytic mechanisms is the lability of the axial pyridine ligands which allows the generation of five- and four-coordinate Co corrole intermediates that can engage in further reactivity.^{6,7,8} The coordinatively unsaturated character of these intermediates also facilitates their attachment to carbon nanotubes⁹ and other nanomaterials, affording nanoconjugates with potentially improved catalytic properties relative to the original molecular catalysts. Somewhat surprisingly, the five-coordinate Co-corrole-pyridine intermediates, $\text{Co}[\text{Cor}](\text{py})$, remain poorly characterized; indeed, except for Co-corrole-triphenylphosphine complexes,^{10,11} which are stable and readily amenable to structural characterization, five-coordinate Co corroles in general remain relatively little explored. In this study, we have investigated the nature of the Co center in $\text{Co}[\text{Cor}](\text{py})$ intermediates, in particular, whether it is low-spin Co(III), intermediate-spin Co(III), or for that matter even Co(II), the last in conjunction with an oxidized corrole²⁻ ligand. Toward this end, we examined two sets of complexes, $\text{Co}[\text{TpXPC}](\text{py})_n$ and $\text{Co}[\text{Br}_8\text{TpXPC}](\text{py})_n$ ($n = 1, 2$, Figure 1), where *TpXPC* denotes a *meso*-tris(*para*-X-phenyl)corrole ligand with $X = \text{CF}_3, \text{H}, \text{Me}, \text{and OMe}$ and Br_8TpXPC the corresponding β -octabrominated ligand. Like $\text{Co}[\text{TPFPC}](\text{py})_2$ [$\text{TPFPC} = \text{meso}$ -tris(pentafluorophenyl)corrole] studied by Gross and coworkers,⁸ the present $\text{Co}[\text{Y}_8\text{TpXPC}](\text{py})_2$ ($Y = \text{H}, \text{Br}$) complexes were found to dissociate essentially completely in dilute dichloromethane solution to afford the five-coordinate complexes $\text{Co}[\text{TpXPC}](\text{py})$. The latter revert back to the six-coordinate forms upon the addition of a small quantity of pyridine. These interconversions are accompanied by dramatic color changes, since the five- and six-coordinate complexes are yellowish-brown and emerald-green in solution, respectively. The two different coordination states thus could be independently characterized with multiple solution-phase analytical tools, as described below.

Results and discussion. (a) Synthesis and proof of composition. The complexes in both the $\text{Co}[\text{TpXPC}](\text{py})_2$ and $\text{Co}[\text{Br}_8\text{TpXPC}](\text{py})_2$ ($X = \text{CF}_3, \text{H}, \text{Me}, \text{OMe}$) series were synthesized via the interaction of the corresponding free-base corroles^{12,13} with Co(II) acetate in pyridine at 100°C over approximately 30 min, followed by column chromatography on silica gel. For chromatographic purification of the β -unsubstituted $\text{Co}[\text{TpXPC}](\text{py})_2$ complexes, it was necessary to include a small amount (~1-2%) of pyridine in the *n*-hexane/dichloromethane

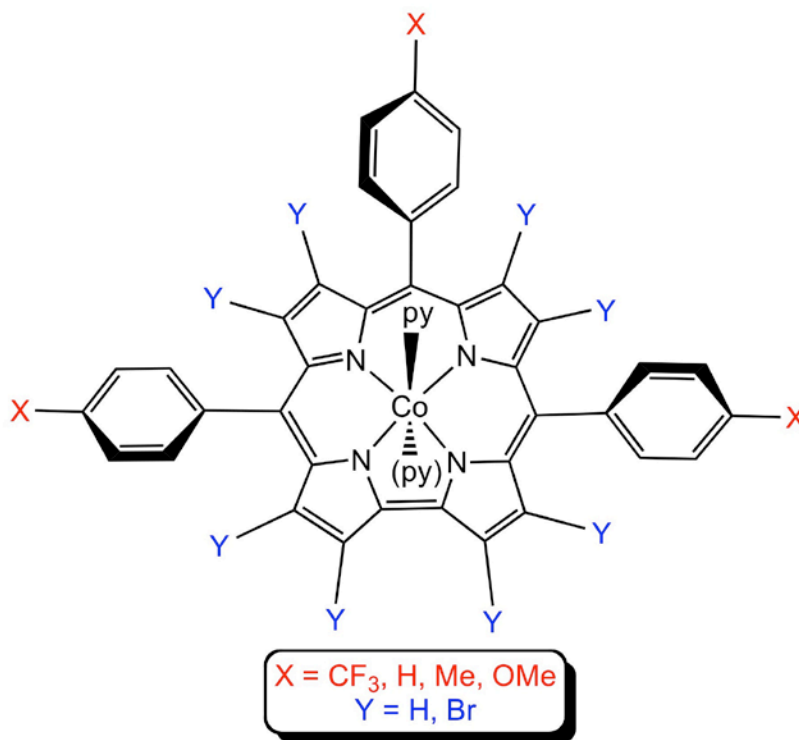


Figure 1. Molecules studied in this work.

eluent mixture, failing which, the complexes underwent severe decomposition in contact with silica. The β -octabrominated complexes proved more stable and could be chromatographed with simply *n*-hexane/dichloromethane as eluent. For long-term stability in solution, however, a small quantity of added pyridine proved essential. For all eight bispyridine complexes, proof of purity came from clean thin-layer chromatograms, electrospray ionization mass spectra, and fully assigned, diamagnetic ^1H NMR spectra, all obtained in the presence of a small quantity of pyridine. Furthermore, X-ray quality crystals were obtained for two of the complexes, $\text{Co}[\text{TpMePC}](\text{py})_2$ and $\text{Co}[\text{Br}_8\text{TpMePC}](\text{py})_2$, by diffusion of methanol vapor into concentrated CH_2Cl_2 or CHCl_3 solutions of the complexes containing a small amount of added pyridine. Again, the presence of added pyridine was crucial. Crystallization in the absence of pyridine led to poor quality crystals of six-coordinate Co isocorrole complexes with a pyridine and a chloride as the axial ligands. Attempts to obtain satisfactory elemental analyses for the bispyridine complexes were also thwarted by the requirement of traces of added pyridine for the stability of the compounds.

Figure 2 depicts the X-ray structures of Co[TpMePC](py)₂ and Co[Br₈TpMePC](py)₂ and Tables 1 and 2 present key crystallographic data and metal-ligand bond distances, respectively. While an essentially planar macrocycle was found for Co[TpMePC](py)₂, the corrole macrocycle in Co[Br₈TpMePC](py)₂ was found to exhibit mild ruffling as well as very slight saddling. The ruffling and saddling dihedrals, as defined earlier,¹⁴ were found to range over 13.7-25.7° and 1.9-5.9°, respectively. Because of the rigidity imposed by the C1-C19 bipyrrrole linkage, corroles are much more resistant to nonplanar distortions than porphyrins, and ruffling, in particular, is energetically very costly.¹⁴ Thus, only a handful of corrole structures are known that are mildly ruffled and none that is strongly ruffled.^{15,16} The Co-N distances involving the corrole nitrogens are particularly short, 1.88 ± 0.03 Å, and those involving the axial pyridines only slightly longer, 1.98 ± 0.01 Å. These distances, which are in excellent accord with literature values for other Co-corrole-bispyridine structures,^{2,5,6,8,17,18,19,20,21} are clearly indicative of a low-spin Co(III) center.

Table 1. Crystallographic data for Co[TpMePC](py)₂ and Co[Br₈TpMePC](py)₂.

Sample	Co[TpMePC](py) ₂ ·2CH ₂ Cl ₂	Co[Br ₈ TpMePC](py) ₂ ·2CHCl ₃
Chemical Formula	C ₅₁ H ₄₁ Cl ₂ CoN ₆	C ₅₂ H ₃₃ Br ₈ N ₆ Cl ₆ Co
Formula mass	867.73	1652.75
Crystal system	Monoclinic	Monoclinic
Space group	<i>P</i> 2 ₁ / <i>n</i>	<i>P</i> 2 ₁ / <i>c</i>
λ (Å)	0.77490	0.7749
<i>a</i> (Å)	18.1623(7)	15.5987(6)
<i>b</i> (Å)	9.7531(4)	20.4468(8)
<i>c</i> (Å)	24.6826(9)	17.4670(7)
α (°)	90	90
β (°)	109.337(2)	96.297(3)
γ (°)	90	90
Z	4	4
<i>V</i> (Å ³)	4125.6(3)	5537.4(4)
Temperature (K)	100(2)	100(2)
ρ (g/cm ³)	1.397	1.982
Measured reflections	65324	67585
Unique reflections	16257	9842
Parameters	551	698
Restraints	1	192
<i>R</i> _{int}	0.0555	0.0519
θ range (°)	2.468 - 37.109	2.113 - 27.555
<i>R</i> 1, <i>wR</i> 2 all data	0.0900, 0.1753	0.0483, 0.1202
<i>S</i> (GooF) all data	1.021	1.026
Max/min res. Dens. (e/Å ³)	1.057/-0.671	1.909/-0.974

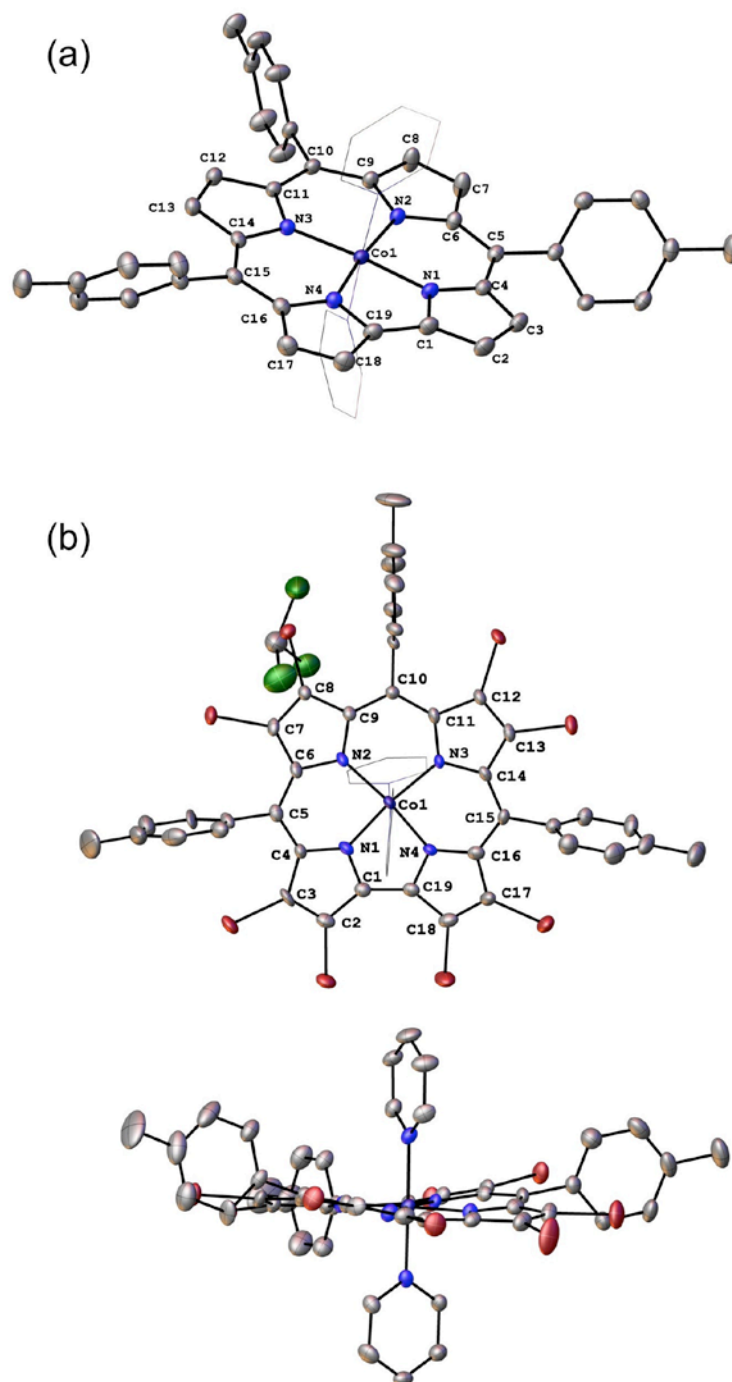


Figure 2. X-ray structures of (a) $\text{Co}[\text{TpMePC}](\text{py})_2$ and (b) $\text{Co}[\text{Br}_8\text{TpMePC}](\text{py})_2$ (top and side views).

Table 2. Selected crystallographic distances (Å) for Co[TpMePC](py)₂ and Co[Br₈TpMePC](py)₂.

Co[TpMePC](py) ₂		Co[Br ₈ TpMePC](py) ₂	
Co(1)-N(1)	1.8675(17)	Co(1)-N(1)	1.889(5)
Co(1)-N(2)	1.9005(17)	Co(1)-N(2)	1.904(5)
Co(1)-N(3)	1.9015(16)	Co(1)-N(3)	1.913(5)
Co(1)-N(4)	1.8689(17)	Co(1)-N(4)	1.877(5)
Co(1)-N(100)	1.9940(16)	Co(1)-N(5)	1.968(5)
Co(1)-N(200)	1.9871(17)	Co(1)-N(6)	1.994(5)

(b) ¹H NMR spectroscopy. Sharp, diamagnetic ¹H NMR spectra could be obtained for the nonbrominated Co[TpXPC](py)₂ series in benzene-*d*₆ even without added pyridine. The axial pyridine hydrogens, which integrated as 4:4:2, were found at relatively high field, as a result of the diamagnetic ring current of the corrole macrocycle. Interestingly, in more polar NMR solvents such as CDCl₃, CD₂Cl₂, and CD₃CN, only very broad and weak signals could be observed, suggesting rapid dissociation and reassociation of the axial pyridines on the NMR time scale. In contrast, freshly prepared²² Co[Br₈TpXPC](py)₂ complexes yielded sharp ¹H NMR spectra even in CDCl₃, attesting to the higher stability of these complexes with respect to dissociation of the axial pyridines.

The chemical shifts of the pyridine protons were found to exhibit some interesting features. Thus, the chemical shifts of the *ortho* protons, which are the most strongly shielded by the corrole's aromatic ring current, were found to undergo a marked downfield shift with increasingly electron-donating character of the *meso*-aryl *para* substituent X. For example, the pyridine *ortho*-H's of Co[TpCF₃PC](py)₂ resonate at 2.54 ppm, whereas those of Co[TpOMePC](py)₂ resonate at 3.70 ppm (Figure 4). Interestingly, the chemical shifts of the pyridine *ortho* protons of the Co[Br₈TpXPC](py)₂ series were found *not* to exhibit a similar substituent dependence. Instead, they were found to exhibit a strong solvent effect. Changing the NMR solvent from CDCl₃ to benzene-*d*₆ result in strong upfield shifts for the *meta* and *para* protons (but not the *ortho* protons). Thus, for Co[Br₈TpOMePC](py)₂, the pyridine *meta*-H's of shift from 5.41 ppm in CDCl₃ to 4.09 benzene-*d*₆, while the same change of solvent shifts the *para*-H's from 6.29 ppm to 4.90 ppm (Figure 5). The reasons underlying these solvent effects are not entirely clear, but stacking interactions involving the axial pyridines and benzene may provide a potential rationale.

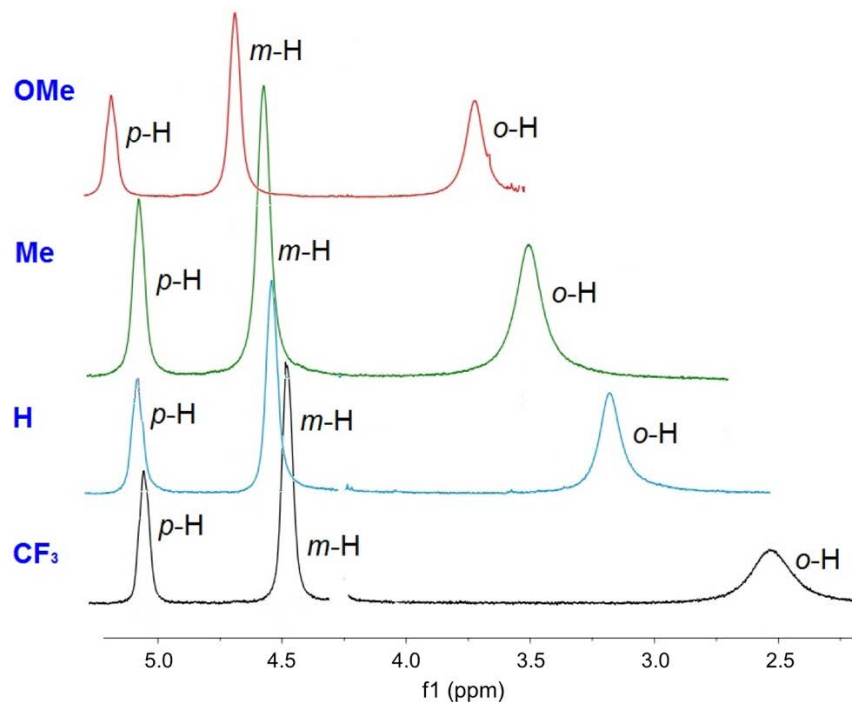


Figure 3. ^1H NMR spectra encompassing the pyridine protons of $\text{Co}[\text{TpXPC}](\text{py})_2$ derivatives; the substituent X is specified in blue.

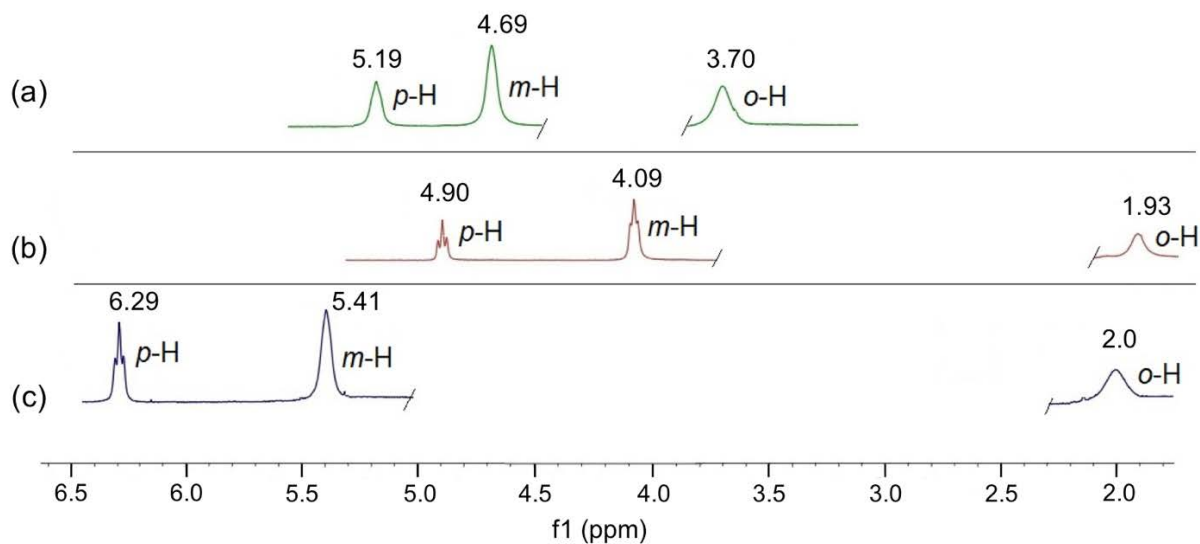


Figure 4. Comparison of ^1H NMR chemical shifts for pyridine protons for $\text{Co}[\text{Y}_8\text{TpOMePC}](\text{py})_2$ ($\text{Y} = \text{H}, \text{Br}$): (a) $\text{Co}[\text{TpOMePC}](\text{py})_2$ in benzene- d_6 , (b) $\text{Co}[\text{Br}_8\text{TpOMePC}](\text{py})_2$ in benzene- d_6 , and (c) $\text{Co}[\text{Br}_8\text{TpOMePC}](\text{py})_2$ in CDCl_3 .

(c) UV-vis spectroscopy. The bispyridine complexes $\text{Co}[\text{TpXPC}](\text{py})_2$ and $\text{Co}[\text{Br}_8\text{TpXPC}](\text{py})_2$, which are very dark green in the solid state, dissolve in noncoordinating solvents such as dichloromethane or chloroform to yield yellowish-brown solutions. Upon addition of a small quantity of pyridine ($\sim 0.5\%$), the solutions turn a brilliant emerald-green, accompanied by dramatic changes in the optical spectra, which include a strongly redshifted Soret band and a greatly intensified Q band (Figure 3 and Table 3). Following earlier studies by Guillard *et. al.*^{6,7} and Gross *et. al.*,⁸ the dark green solutions are most reasonably assigned to the six-coordinate bispyridine complexes, whereas the main chromophore in the brown solutions is thought to be the five-coordinate $\text{Co}[\text{Cor}](\text{py})$ form.

A key motivation for studying the two series of complexes with varying *meso*-aryl *para* substituents was to examine substituent effects on their Soret maxima, which can shed light on the innocence or noninnocence of the corrole macrocycle, an expectation that proved amply rewarded. Over a long series of studies,²³ we have shown that Soret maxima of innocent metallocorroles, such as CrO and MoO corroles,²⁴ TcO^{25} and ReO^{26} corroles, RuN^{27} and OsN^{28} corroles, and $\text{Au}^{29,30,31}$ corroles, are insensitive to the *meso*-aryl *para* substituent X. In contrast, the Soret maxima of noninnocent metallocorroles, of which Mn ,³² Fe ,^{32,33,34,35,36,37} Cu ,^{38,39,40,41,42,43,44,45,46} and certain Pt^{47} corroles provide salient examples, undergo marked redshifts with increasing electron-donating character of the substituent X. As shown in Figure 3 and Table 3, we encounter both behaviors in this study. Thus, the Soret maxima of the bispyridine complexes, $\text{Co}[\text{TpXPC}](\text{py})_2$, are largely insensitive to X consistent with an innocent low-spin- Co^{III} -corrole³⁻ electronic description. In contrast, in the absence of added pyridine, the Soret maxima of the brown solutions containing five-coordinate $\text{Co}[\text{TpXPC}](\text{py})$ complexes redshift monotonically with increasing electron-donating character of X, shifting from 386 nm for X = CF_3 to 402 nm for X = OMe , suggesting a noninnocent Co^{II} -corrole^{•2-}-like formulation.

Table. 3. Soret maxima (nm) for the Co complexes studied.

Series	Solvent	<i>para</i> -substituent X			
		CF_3	H	Me	OMe
$\text{Co}[\text{TpXPC}](\text{py})$	CH_2Cl_2	386	388	393	402
$\text{Co}[\text{Br}_8\text{TpXPC}](\text{py})$	CH_2Cl_2	396	392	391	392
$\text{Co}[\text{TpXPC}](\text{py})_2$	$\text{CH}_2\text{Cl}_2 + 0.5\% \text{ py}$	442, 453 (sh)	437, 452	437, 453	434, 453
$\text{Co}[\text{Br}_8\text{TpXPC}](\text{py})_2$	$\text{CH}_2\text{Cl}_2 + 0.5\% \text{ py}$	447, 460	445, 461	445, 461	446, 462

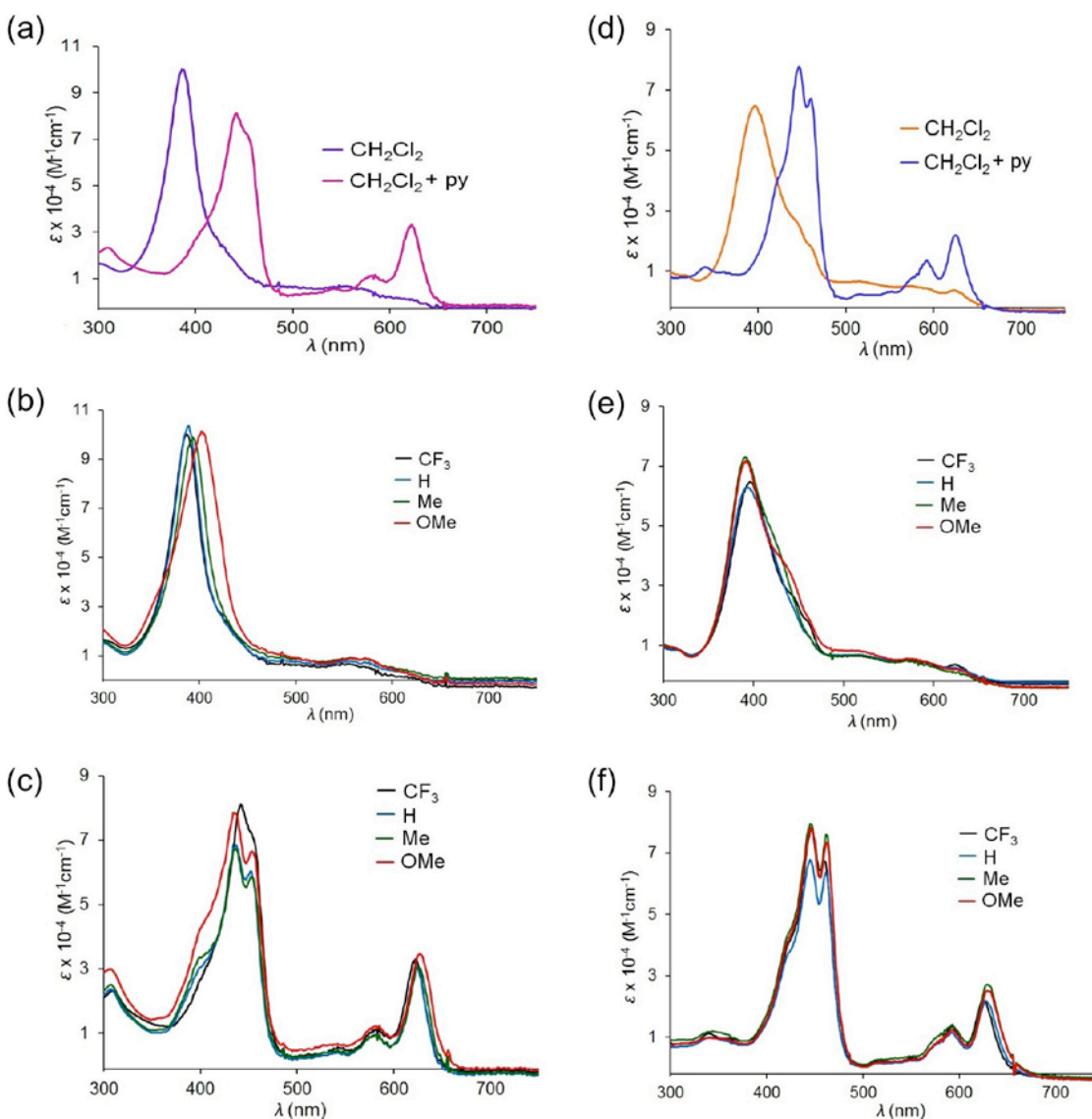


Figure 5. UV-vis spectra of (a) $\text{Co}[\text{TpCF}_3\text{PC}](\text{py})_2$, (b) the $\text{Co}[\text{TpXPC}](\text{py})_2$ series in CH_2Cl_2 , (c) the $\text{Co}[\text{TpXPC}](\text{py})_2$ series in CH_2Cl_2 with 0.5% pyridine, (d) $\text{Co}[\text{Br}_8\text{TpCF}_3\text{PC}](\text{py})_2$, (e) the $\text{Co}[\text{Br}_8\text{TpXPC}](\text{py})_2$ series in CH_2Cl_2 , (f) the $\text{Co}[\text{Br}_8\text{TpXPC}](\text{py})_2$ series in CH_2Cl_2 with 0.5% pyridine.

Interestingly, for the β -octabrominated $\text{Co}[\text{Br}_8\text{TpXPC}](\text{py})_2$ series, the Soret maxima are relatively invariant with respect to the substituent X even in neat CH_2Cl_2 . Although it is tempting to interpret this observation as suggesting a relatively innocent octabromocorrole ligand in the five-coordinate monopyridine complexes, we believe that that is in fact not the case. TDDFT studies on Cu corroles suggest that the key substituent-sensitive feature under the Soret envelope

consists of one or more aryl-to-corrole^{•2-} charge transfer transitions.⁴⁸ For planar β -octabromo-*meso*-triarylcorrole complexes, steric inhibition of resonance is thought to inhibit such transitions, thus providing a rationale for the relative substituent-insensitivity of the Soret maxima. A similar difference in behavior between the *TpXPC* and *Br₈TpXPC* has also been noted for FeNO corroles, which are also believed to be noninnocent.³⁶

(d) DFT calculations. DFT calculations have long provided a qualitatively excellent description of ligand noninnocence in metalloporphyrin and metallocorrole systems.^{49,50} Here as well, all-electron B3LYP-D3/STO-TZP calculations on Co[TPC](py) (TPC = *meso*-triphenylcorrole, i.e., *TpXPC* with X = H) afforded compelling support for the Co^{II}-corrole^{•2-} formulation of the five-coordinate monopyridine complexes. The use of a C_s symmetry constraint allowed us to evaluate three different solutions, a broken-symmetry $M_S = 0$ solution and two $M_S = 1$ solutions with A' and A'' symmetry. The ground state was found to correspond to the $M_S = 0$ solution (S_0). An examination of the valence MOs and broken-symmetry spin density profile clearly revealed a Co(II) center antiferromagnetically coupled to a corrole radical via a Co(d_{z^2})-corrole(“ a_{2u} ”) orbital interaction (Figure 6). It is worth noting that this orbital interaction is very common for five-coordinate first-row transition metal corroles and in particular has been noted for MnCl,³² FeCl,³² and FeNO^{35,36} corroles. The lowest triplet state (T_1), at an energy of 0.13 eV relative to the ground state, turned out to be not the corresponding ferromagnetically coupled state, but rather an intermediate-spin Co(III) state with a $d_{xy}^2 d_{xz}^2 d_{yz}^1 d_{z^2}^1$ electronic configuration, where the Co(d_{yz}) orbital transforms as a'' under C_s symmetry. Another intermediate-spin Co(III) state with a $d_{xy}^2 d_{xz}^1 d_{yz}^2 d_{z^2}^1$ electronic configuration (T_2) was found to be only 0.09 eV higher than T_1 .

(e) EPR spectroscopy. Solutions of Co[*TpXPC*](py)₂ (X=H, Me) and Co[*Br₈TpXPC*](py)₂ (X=H, Me) in 2:1 CH₂Cl₂/toluene, where the five-coordinate monopyridine forms are expected to dominate, all yielded similar X-band EPR spectra at room temperature (SI, Fig. S25). In all cases, they were centered around $g = 2$, moderately broad (FWHH ≈ 50 G), and devoid of resolvable hyperfine interactions, as expected for strongly delocalized spin systems. The room-temperature solution spectra exhibited distinct inflection points, consistent with a slightly split triplet and/or a narrow distribution of g -values. In frozen glasses at low temperature ($T = 69$ -125 K), the inflection points were smeared out, suggesting that they result from slight anisotropies rather than unresolved hyperfine couplings. (Figure 7).

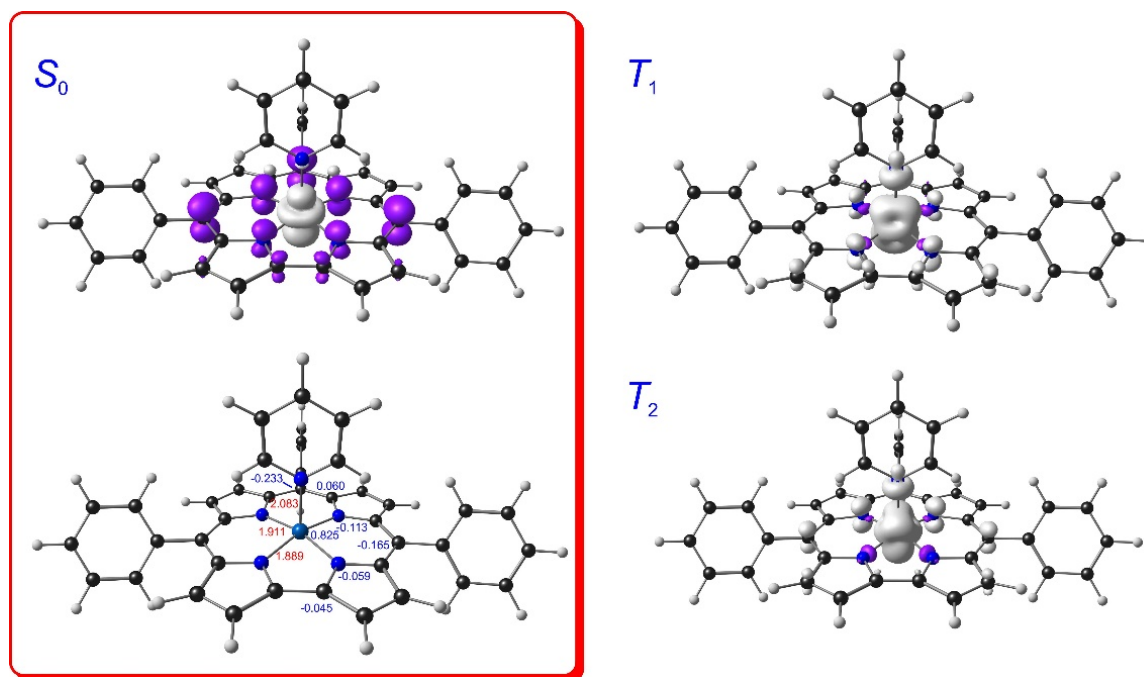


Figure 6. Inset: Broken-symmetry spin density plot (contour $0.005 \text{ e}/\text{\AA}^3$), Mulliken spin populations, and skeletal bond distances (\AA) for the S_0 ground state. Also shown are spin density plots for the T_1 and T_2 states.

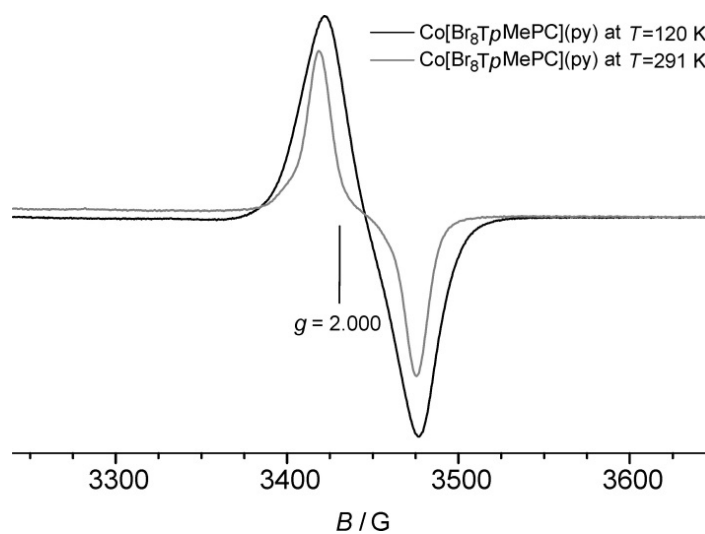


Figure 7. Solution and solid-state (frozen-glass) X-band EPR spectra of $\text{Co}[\text{Br}_8\text{TpMePC}](\text{py})$. Modulation 1 G; microwave power 63 mW. The relative intensities are arbitrary.

For the frozen-glass samples, the EPR signal intensities were found to increase with temperature, contrary to what would be expected for a relaxation-broadened Co-centered system. The temperature variation for the frozen solution of Co[Br₈TpMePC](py) could be modeled with a Boltzmann expression (see Figure S26 in SI), assuming an EPR-silent ground state and a triplet state ~0.01 eV higher in energy. Although this singlet-triplet gap is smaller than that obtained from the calculations, the overall picture of a singlet ground state with thermally accessible triplet states is corroborated.

(f) Electrochemistry.⁵¹ The complexes synthesized were also examined with cyclic voltammetry with the goal of obtaining additional insight into the nature of the five-coordinate monopyridine complexes. Measurements in dichlororomethane without added pyridine generally revealed two reversible oxidations and two quasireversible or irreversible reductions. The relatively high first reduction potentials, ~ -0.32 ± 0.04 V for Co[TpXPC](py) and -0.06 ± 0.03 V for Co[Br₈TpXPC](py), are consistent with a Co^{II}(py)-corrole^{•2-}/Co^{II}(py)-corrole³⁻ reduction (Figure 8 and Table 4). In the presence of 0.5% pyridine, however, the reductions proved complex, reversible in some cases and irreversible for others, and generally not interpretable in the absence of additional spectroscopic studies. Interestingly, the presence of pyridine led to only small changes in the first oxidation potentials. Following Kadish and coworkers,⁷ the first oxidations of the bispyridine complexes are expected to be corrole-centered, i.e., Co^{III}(py)₂-Cor³⁻ → Co^{III}(py)₂-Cor^{•2-}. It is not unreasonable, in our view, that oxidation of the five-coordinate monopyridine complexes, i.e., the Co^{II}(py)-corrole^{•2-} → [Co^{III}(py)-corrole^{•2-} ↔ Co^{II}(py)-corrole⁻] process, occurs at approximately the same potential.

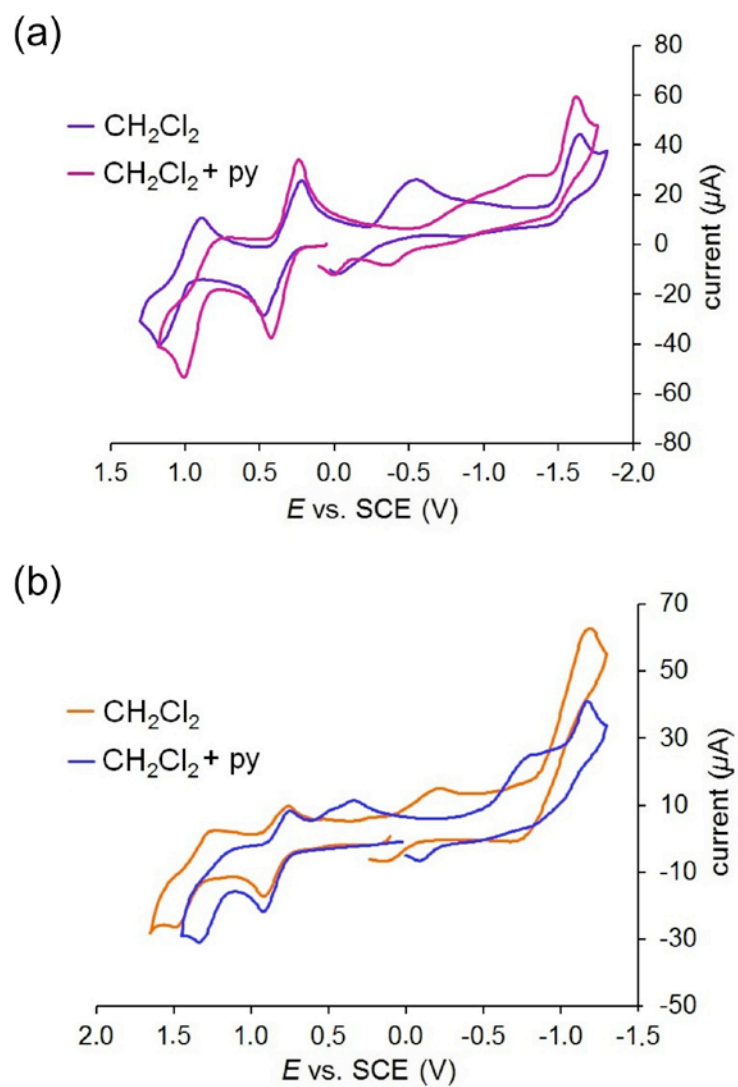


Figure 8. Cyclic voltammograms of (a) Co[TpCF₃PC](py)₂ and (b) Co[Br₈TpCF₃PC](py)₂ in different solvents, each with 0.1 M TBAP. Scan rate: 0.1 V/s.

Table 4. Redox potentials of the complexes synthesized in two different solvent systems

Series	X	E_{ox2}	E_{ox1}	E_{red1}	E_{red2}
Co[<i>TpXPC</i>](py) ₂ in CH ₂ Cl ₂	CF ₃	1.03	0.35	-0.28	-1.64
	H	0.93	0.24	-0.31	-1.70
	Me	0.89	0.22	-0.33	-1.73
	OMe	0.82	0.18	-0.36	-1.78
Co[<i>TpXPC</i>](py) ₂ in CH ₂ Cl ₂ with 1% py	CF ₃	0.86	0.33	-0.36 ^a	-1.62
	H	0.78	0.19	-0.44 ^a	-1.75
	Me	0.76	0.14	-0.46 ^a	-1.74
	OMe	0.74	0.12	-0.43 ^a	-1.81
Co[Br ₈ <i>TpXPC</i>](py) ₂ in CH ₂ Cl ₂	CF ₃	1.38	0.83	-0.04	-1.19
	H	1.32	0.71	-0.06	-1.20
	Me	1.29	0.67	-0.07	-1.23
	OMe	1.21	0.67	-0.09	-1.27
Co[Br ₈ <i>TpXPC</i>](py) ₂ in CH ₂ Cl ₂ with 1% py	CF ₃	1.33	0.83	-0.09 ^a	-1.18
	H	1.22	0.69	-0.21 ^a	-1.21
	Me	1.22	0.67	-0.21 ^a	-1.27
	OMe	1.19	0.66	-0.19 ^a	-1.32

^a peak potential during anodic sweep

Conclusion. Our X-ray crystallographic and ¹H NMR studies have confirmed that Co-triarylcorrole-bispyridine complexes are authentic Co(III) complexes, as long supposed. More interestingly, substituent effects on the Soret maxima and broken-symmetry DFT calculations strongly support a Co^{II}-corrole²⁻ formulation for the corresponding five-coordinate monopyridine complexes. Such a ground state corresponds to an antiferromagnetically coupled, open-shell singlet, where a Co(d₂₂)-corrole(“a_{2u}”) orbital overlap mediates the metal-ligand spin coupling. The calculations also predict low-energy, potentially thermally accessible triplet states with intermediate-spin Co(III) centers, a scenario that has been experimentally corroborated with EPR spectroscopy. The study underscores – yet again²³ – the broad prevalence of ligand noninnocence among first-row transition metal corrole derivatives.

Experimental section

Materials. All reagents and solvents were used as purchased unless otherwise noted. Silica gel 150 (35-70 μm particle size, Davisil) was used as the stationary phase for flash chromatography and silica gel 60 preparative thin-layer chromatographic (PLC) plates (20 x 20 cm, 0.5 mm thick, Merck) were used for final purification of the products. CHROMASOLV® HPLC-grade *n*-hexane and dichloromethane were used as solvents for column chromatography. For electrochemical measurements, anhydrous dichloromethane was predried with CaH_2 and stored over 3Å molecular sieves prior to distillation. Tetrakis(*n*-butyl)ammonium perchlorate (Sigma-Aldrich, TBAP), recrystallized three times from absolute ethanol, vacuum-dried at 40°C for two days, and stored in a desiccator for at least two weeks, was used as the supporting electrolyte. The starting materials, free-base corroles $\text{H}_3[\text{TpXPC}]^{12}$ and free-base β -octabromocorroles $\text{H}_3[\text{Br}_8\text{TpXPC}]^{52,13}$ (X = CF_3 , H, Me, OMe), were synthesized as previously reported.⁵³ Cobalt(II) acetate tetrahydrate (Merck) and pyridine ($\geq 99\%$, Sigma-Aldrich) were both used as received.

Instrumentation. UV-vis spectra were recorded on an Agilent Cary 8454 UV-Visible spectrophotometer in CH_2Cl_2 . Cyclic voltammetry experiments were performed with an EG&G Princeton Applied Research Model 263A potentiostat equipped with a three-electrode system consisting of a glassy carbon working electrode, a platinum wire counterelectrode, and a saturated calomel reference electrode (SCE). The reference electrode was separated from bulk solution by a fritted-glass bridge filled with the solvent/supporting electrolyte mixture. All potentials were referenced to the SCE. A scan rate of 100 mV/s was used. The anhydrous dichloromethane solutions were purged with argon for at least 5 min prior to electrochemical measurements and an argon blanket was maintained over the solutions during the measurements. X-band EPR spectra were recorded with a Bruker Elexsys E500 equipped with a Bruker ER 4116 DM dual-mode cavity, an EIP 538B frequency counter and an ER035M NMR gaussmeter. Low-temperature measurements were conducted by use of an Oxford Instruments Mercury iTC temperature controller, using liq. N_2 as a coolant. Pumping allowed a base temperature of 69 K. ^1H NMR spectra were recorded at room temperature on a 400 MHz Bruker Avance III HD spectrometer equipped with a 5 mm BB/ ^1H (BB = ^{19}F , ^{31}P - ^{15}N) SmartProbe in CDCl_3 and C_6D_6 . High resolution electrospray ionization (HR-ESI) mass spectra were obtained on an LTQ Orbitrap XL spectrometer.

Synthesis of cobalt-triarylcorrole-bispyridine complexes. A detailed procedure is described below for Co[*Tp*CF₃PC](py)₂. A similar procedure was also followed for synthesis of the other Co[*Tp*XPC](py)₂ complexes, except for details of the chromatographic purifications, which are specified below.

Synthesis of Co[*Tp*CF₃PC](py)₂. A 50-mL round-bottom flask equipped with a magnetic stir-bar was charged with free-base tris(4-trifluoromethylphenyl)corrole (0.035 g, 0.048 mmol) dissolved in pyridine (10 mL). To this solution was added 10 equiv of Co(OAc)₂•4H₂O (0.12 g, 0.48 mmol). The reaction flask was then fitted with a reflux condenser and heated on an oil bath at 100°C with stirring for 25-30 min, whereupon completion of metal insertion was confirmed by UV-vis spectroscopy and/or mass spectrometry. Upon cooling, the solution was rotary evaporated to dryness under high vacuum to yield. The resulting dark greenish-brown residue was redissolved in a minimum volume of dichloromethane containing a couple of drops of pyridine and chromatographed on a silica gel column (10 cm in height) with *n*-hexane/dichloromethane/pyridine (2:1:0.02, subsequently 1:1:0.02) as eluent. The front-running, emerald-green band was collected and identified as the title compound. Recrystallization from a mixture of 3:1 *n*-hexane/dichloromethane with a few drops of pyridine afforded the pure product (0.04 g, 0.042 mmol, 87.5%). UV-vis (CH₂Cl₂) λ_{max} [nm, ε x 10⁻⁴ (M⁻¹cm⁻¹): 386 (10.02). UV-vis (CH₂Cl₂, 0.5% pyridine) λ_{max} [nm, ε x 10⁻⁴ (M⁻¹cm⁻¹): 442 (8.13), 453 (sh) (7.24), 582 (1.14), 623 (3.31). ¹H NMR (benzene-*d*₆, 25°C) δ: 9.24 (d, *J* = 4.1 Hz, 2H, β-pyrrolic), 9.01 (d, *J* = 4.1 Hz, 2H, β-pyrrolic), 8.82-8.72 (m, 4H, β-pyrrolic), 8.26 (d, *J* = 7.9 Hz, 4H, 5,15-*o/m*-aryl), 8.17 (d, *J* = 7.9 Hz, 2H, 10-*o/m*-aryl), 7.75 (d, *J* = 8.0 Hz, 4H, 5,15-*o/m*-aryl), 7.70 (d, *J* = 8.1 Hz, 2H, 10-*o/m*-aryl), 5.06 (s, 2H, *p*-H of pyridine), 4.49 (s, 4H, *m*-H of pyridine), 2.54 (br s, 4H, *o*-H of pyridine). HRMS (major isotopomers in presence of a drop of pyridine, M = C₄₀H₂₀N₄F₉Co): [M]⁺ (0.35) 786.0802 (expt), 786.0871 (calcd); [M + py]⁺ (1.00) 865.1284 (expt), 865.1294 (calc); [M + 2 py]⁺ (0.90) 944.1715 (expt), 944.1715 (calc).

Synthesis of Co[TPC](py)₂. Silica gel column chromatography with 1:1:0.02 *n*-hexane/dichloromethane/pyridine as eluent followed by recrystallization from 3:1 *n*-hexane/CH₂Cl₂ with a few drops of pyridine afforded the pure product (0.038 g, 0.051 mmol, 77%). UV-vis (CH₂Cl₂) λ_{max} [nm, ε x 10⁻⁴ (M⁻¹cm⁻¹): 388 (10.35). UV-vis (CH₂Cl₂, 0.5% pyridine) λ_{max} [nm, ε x 10⁻⁴ (M⁻¹cm⁻¹): 437 (6.86), 452 (6.03), 582 (0.95), 623 (3.09). ¹H NMR (benzene-*d*₆, 25°C) δ: 9.05 (d, *J* = 4.3 Hz, 2H, β-pyrrolic), 8.93 (d, *J* = 4.6 Hz, 2H, β-pyrrolic), 8.76-8.70 (m, 4H, β-pyrrolic), 8.40-8.35 (m, 4H, 5,15-*o/m*-aryl), 8.30-8.25 (m, 2H, 10-*o/m*-aryl),

7.53-7.41 (m, 9H, 5,15, & 10-*o/m/p*-aryl), 5.08 (s, 2H, *p*-H of pyridine), 4.54 (s, 4H, *m*-H of pyridine), 3.18 (br s, 4H, *o*-H of pyridine). HRMS (major isotopomers in presence of a drop of pyridine, M = C₃₇H₂₃N₄Co): [M]⁺ (0.70) 582.1225 (expt), 582.1249 (calc); [M + py]⁺ (1.00) 661.1676 (expt), 661.1671 (calc); [M + 2 py]⁺ (0.30) 740.2100 (expt), 740.2093 (calc).

Synthesis of Co[TpMePC](py)₂. Silica gel column chromatography with 1:1:0.02 *n*-hexane/dichloromethane/pyridine as eluent followed by recrystallization from 3:1 *n*-hexane/CH₂Cl₂ with a few drops of pyridine afforded the pure product (0.0395 g, 0.05 mmol, 82%). UV-vis (CH₂Cl₂) λ_{max} [nm, ε x 10⁻⁴ (M⁻¹cm⁻¹): 393 (9.90). UV-vis (CH₂Cl₂, 0.5% pyridine) λ_{max} [nm, ε x 10⁻⁴ (M⁻¹cm⁻¹): 437 (6.73), 453 (5.87), 581 (0.96), 625 (3.05). ¹H NMR (benzene-*d*₆, 25°C) δ: 8.96 (d, *J* = 4.3 Hz, 2H, β-pyrrolic), 8.86 (d, *J* = 4.7 Hz, 2H, β-pyrrolic), 8.69 (d, *J* = 4.6 Hz, 2H, β-pyrrolic), 8.65 (s, 2H, β-pyrrolic), 8.28 (d, *J* = 7.8 Hz, 4H, 5,15-*o/m*-aryl), 8.20 (d, *J* = 7.8 Hz, 2H, 10-*o/m*-aryl), 7.31-7.22 (m, 6H, 5,15, & 10-*o/m*-aryl), 5.08 (s, 2H, *p*-H of pyridine), 4.57 (s, 4H, *m*-H of pyridine), 3.51 (br s, 4H, *o*-H of pyridine), 2.31 (overlapping s, 9H, 5,10,15-Me). HRMS (major isotopomers in presence of a drop of pyridine, M = C₄₀H₂₉N₄Co): [M]⁺ (0.80) 624.1691 (expt), 624.1719 (calc); [M + py]⁺ (1.00) 703.2148 (expt), 703.2141 (calc); [M + 2 py]⁺ (0.25) 782.2572 (expt), 782.2563 (calc).

X-ray quality crystals were obtained by diffusion of methanol vapour over one week into a concentrated CH₂Cl₂ solution of the complex containing few drops of pyridine.

Synthesis of Co[TpOMePC](py)₂. Silica gel column chromatography with 2:3:0.025 *n*-hexane/dichloromethane/pyridine as eluent followed by recrystallization from 2:1 *n*-hexane/CH₂Cl₂ with a few drops of pyridine afforded the pure product (0.0393 g, 0.047 mmol, 83.5%). UV-vis (CH₂Cl₂) λ_{max} [nm, ε x 10⁻⁴ (M⁻¹cm⁻¹): 402 (10.13). UV-vis (CH₂Cl₂, 0.5% pyridine) λ_{max} [nm, ε x 10⁻⁴ (M⁻¹cm⁻¹): 434 (7.87), 453 (6.66), 582 (1.23), 627 (3.47). ¹H NMR (benzene-*d*₆, 25°C) δ: 9.0 (d, *J* = 4.2 Hz, 2H, β-pyrrolic), 8.91 (d, *J* = 4.6 Hz, 2H, β-pyrrolic), 8.76 (d, *J* = 4.3 Hz, 2H, β-pyrrolic), 8.70 (s, 2H, β-pyrrolic), 8.29 (d, *J* = 8.3 Hz, 4H, 5,15-*o/m*-aryl), 8.22 (d, *J* = 8.3 Hz, 2H, 10-*o/m*-aryl), 7.13-7.04 (m, 6H, 5,15, & 10-*o/m*-aryl), 5.19 (s, 2H, *p*-H of pyridine), 4.69 (s, 4H, *m*-H of pyridine), 3.70 (broad-s, 4H, *o*-H of pyridine), 3.49 (overlapping s, 9H, 5,10,15-OMe). HRMS (major isotopomers in presence of a drop of pyridine, M = C₄₀H₂₉N₄O₃Co): [M]⁺ (1.00) 672.1536 (expt), 672.1566 (calc); [M + py]⁺ (1.00) 751.1989 (expt), 751.1988 (calc); [M + 2 py]⁺ (0.25) 830.2414 (expt), 830.2410 (calc).

Synthesis of cobalt-β-octabromocorrole-bispyridine complexes. A detailed procedure is described below for Co[Br₈TpMePC](py)₂; the other β-octabromocorrole complexes were

synthesized via a similar protocol, except for the optimum chromatographic purification, which is indicated separately for each complex.

Synthesis of Co[Br₈TpMePC](py)₂. A 50 mL round-bottomed flask equipped with a magnetic stir-bar was charged with free-base tris(4-trimethylphenyl)corrole (0.025 g, 0.021 mmol) dissolved in pyridine (8-10 mL). To this solution was added 6 equiv of Co(OAc)₂•4H₂O (0.0314 g, 0.126 mmol) The reaction flask was then fitted with a reflux condenser and heated on an oil bath at 100°C with stirring for 30 min, whereupon completion of metal insertion was confirmed by UV-Vis spectroscopy and mass spectrometry. Upon cooling, the solution was rotary evaporated under high vacuum to yield a dark brown residue. The residue was redissolved in a minimum volume of dichloromethane and was chromatographed on a silica gel column (length 12 cm) with 3:1 *n*-hexane/dichloromethane as eluent. The product eluted as a greenish-brown band, which was collected and evaporated to dryness. Final purification was carried out with PLC using 2:1 *n*-hexane/CH₂Cl₂ as eluent. The front brown band contained pure product Co[Br₈TpMePC](py)₂ (0.0214g, 0.015 mmol, 71.4%). UV-vis (CH₂Cl₂) λ_{max} [nm, ε x 10⁻⁴ (M⁻¹cm⁻¹)]: 391 (7.31). UV-vis (CH₂Cl₂, 0.5% pyridine) λ_{max} [nm, ε x 10⁻⁴ (M⁻¹cm⁻¹)]: 445 (7.94), 461 (7.60), 593 (1.41), 629 (2.71). ¹H NMR (CDCl₃, 25°C) δ: 7.62 (d, *J* = 7.8 Hz, 4H, 5,15-*o/m*-aryl), 7.56 (d, *J* = 7.8 Hz, 2H, 10-*o/m*-aryl), 7.43 (d, *J* = 7.7 Hz, 4H, 5,15-*o/m*-aryl), 7.35 (d, *J* = 7.8 Hz, 2H, 10-*o/m*-aryl), 6.30 (s, 2H, *p*-H of pyridine), 5.44 (s, 4H, *m*-H of pyridine), 2.67 (s, 6H, 5,15-Me protons), 2.62 (s, 3H, 10-Me), 2.07 (broad-s, 4H, *o*-H of pyridine). HRMS (major isotopomer in the presence of a drop of pyridine, M = C₄₀H₂₁N₄Br₈Co): [M + 2py + H]⁺ 1414.5393 (expt), 1414.5410 (calc).

X-ray quality crystals were obtained by diffusion of methanol vapour over several days into a concentrated CHCl₃ solution of the complex containing few drops of pyridine.

Synthesis of Co[Br₈TPC](py)₂. Silica gel column chromatography with 2:1 *n*-hexane/CH₂Cl₂ followed by PLC with 3:2 *n*-hexane/CH₂Cl₂ as eluent afforded pure Co[Br₈TPC](py)₂ (0.0233 g, 0.017 mmol, 77%). UV-vis (CH₂Cl₂) λ_{max} [nm, ε x 10⁻⁴ (M⁻¹cm⁻¹)]: 392 (6.29). UV-vis (CH₂Cl₂, 0.5% pyridine) λ_{max} [nm, ε x 10⁻⁴ (M⁻¹cm⁻¹)]: 445 (6.78), 461 (6.37), 593 (1.15), 628 (2.17). ¹H NMR (CDCl₃, 25°C) δ: 7.79-7.66 (m, 9H, *meso*-aryl), 7.62 (t, *J* = 7.5 Hz, 4H, 5,15-*o/m*-aryl), 7.57-7.52 (m, 2H, 10-*o/m*-aryl), 6.29 (t, *J* = 7.1 Hz, 2H, *p*-H of pyridine), 5.41 (s, 4H, *m*-H of pyridine), 1.89 (br s, 4H, *o*-H of pyridine). HRMS (major isotopomer in the presence of a drop of pyridine, M = C₃₇H₁₅N₄Br₈Co): [M + 2py + H]⁺ 1372.4912 (expt), 1372.4937 (calc).

Synthesis of Co[Br₈TpOMePC](py)₂. Silica gel column chromatography with 1:2 *n*-hexane/CH₂Cl₂ followed by PLC with 3:7 *n*-hexane/CH₂Cl₂ as eluent afforded pure Co[Br₈TpOMePC](py)₂ (0.0217 g, 0.0148 mmol, 74.2%). UV-vis (CH₂Cl₂) λ_{\max} [nm, $\epsilon \times 10^{-4}$ (M⁻¹cm⁻¹): 392 (7.19). UV-vis (CH₂Cl₂, 0.5% pyridine) λ_{\max} [nm, $\epsilon \times 10^{-4}$ (M⁻¹cm⁻¹): 446 (7.83), 462 (7.34), 593 (1.26), 629 (2.50). ¹H NMR (CDCl₃, 25°C) δ : 7.63 (d, *J* = 8.3 Hz, 4H, 5,15-*o/m*-aryl), 7.58 (d, *J* = 8.4 Hz, 2H, 10-*o/m*-aryl), 7.17 (d, *J* = 8.4 Hz, 4H, 5,15-*o/m*-aryl), 7.10 (d, *J* = 8.4 Hz, 2H, 10-*o/m*-aryl), 6.29 (t, *J* = 7.1 Hz, 2H, *p*-H of pyridine), 5.41 (s, 4H, *m*-H of pyridine), 4.06 (s, 6H, 5,15-OMe), 4.03 (s, 3H, 10-OMe), 2.0 (br s, 4H, *o*-H of pyridine). HRMS (major isotopomer in the presence of a drop of pyridine, M = C₄₀H₂₁N₄Br₈O₃Co): [M + 2py + H]⁺ 1462.5242 (expt), 1462.5254 (calc).

Synthesis of Co[Br₈TpCF₃PC](py)₂. Silica gel column chromatography with 3:1 *n*-hexane/CH₂Cl₂ followed by PLC with 2:1 *n*-hexane/CH₂Cl₂ as eluent afforded pure Co[Br₈TpCF₃PC](py)₂ (0.0223 g, 0.01415 mmol, 78.6%). UV-vis (CH₂Cl₂) λ_{\max} [nm, $\epsilon \times 10^{-4}$ (M⁻¹cm⁻¹): 396 (6.48). UV-vis (CH₂Cl₂, 0.5% pyridine) λ_{\max} [nm, $\epsilon \times 10^{-4}$ (M⁻¹cm⁻¹): 447 (7.79), 460 (6.72), 593 (1.36), 625 (2.19). ¹H NMR (CDCl₃, 25°C) δ : 7.92-7.81 (m, 12H, *meso*-aryl), 6.31 (t, *J* = 7.2 Hz, 2H, *p*-H of pyridine), 5.42 (s, 4H, *m*-H of pyridine). HRMS (major isotopomer in the presence of a drop of pyridine, M = C₄₀H₁₂N₄Br₈F₉Co): [M + 2py + H]⁺ 1575.4503 (expt), 1575.4484(calc).

Crystal Structure Determination. X-ray diffraction data were collected on beamline 11.3.1 at the Advanced Light Source, Lawrence Berkeley National Laboratory, using a Bruker D8 diffractometer equipped with a PHOTON100 CMOS detector operating in shutterless mode. The crystal, coated in protective oil, was mounted on a MiTeGen[®] kapton micromount and placed under a nitrogen stream at 100(2) K provided by an Oxford Cryostream 800 Plus low-temperature apparatus. Diffraction data were collected using synchrotron radiation monochromated using silicon(111) to a wavelength of 0.7749(1)Å. An approximate full-sphere of data was collected using a combination of phi and omega scans with scan speeds of 4° per second for the phi scans and 1 degree per second for the omega scans at 2 θ = 0 and -45, respectively. The structures were solved by intrinsic phasing (SHELXT)⁵⁴ and refined by full-matrix least squares on *F*² (SHELXL-2014).⁵⁵ All non-hydrogen atoms were refined anisotropically. Hydrogen atoms were geometrically calculated and refined as riding atoms. Additional crystallographic information has been summarized in Table 1 and 2 and full details can be found in the crystallographic information files provided as Supplementary Information.

Computational methods. All DFT calculations were carried with the B3LYP^{56,57} exchange-correlation functional (20% Hartree-Fock exchange), in conjunction with Grimme's D3 dispersion correction,⁵⁸ and all electron STO-TZP basis sets, as implemented in the ADF 2014 program system.⁵⁹

Supporting Information Available. ¹H NMR spectra, mass spectra, EPR spectra, and B3LYP/STO-TZP optimized coordinates (19 pages).

Acknowledgements. This work was supported by grants 231086 and 262229 of the Research Council of Norway (AG), the National Research Fund of the Republic of South Africa (JC) and by the Advanced Light Source, Berkeley, California (KJG, LJM). The Advanced Light Source is supported by the Director, Office of Science, Office of Basic Energy Sciences, of the U.S. Department of Energy under Contract No. DE-AC02-05CH11231.

References

-
- ¹ Lemon, C. M.; Dogutan, D. K.; Nocera, D. G. Porphyrin and Corrole Platforms for Water Oxidation, Oxygen Reduction, and Peroxide Dismutation. *In Handbook of Porphyrin Science*. Kadish, K. M.; Smith, K. M.; Guillard, R. (eds). 2012, vol. 21, pp. 1–143. DOI: 10.1142/9789814397605_0001.
- ² Mondal, B.; Sengupta, K.; Rana, A.; Mahammed, A.; Botoshansky, M.; Dey, S. G.; Gross, Z.; Dey, A. Cobalt Corrole Catalyst for Efficient Hydrogen Evolution Reaction from H₂O under Ambient Conditions: Reactivity, Spectroscopy, and Density Functional Theory Calculations. *Inorg. Chem.* **2013**, *52*, 3381-3387.
- ³ Mahammed, A.; Mondal, B.; Rana, A.; Dey, A.; Gross, Z. The Cobalt Corrole Catalyzed Hydrogen Evolution Reaction: Surprising Electronic Effects and Characterization of key Reaction Intermediates. *Chem. Commun.* **2014**, *50*, 2725-2727.
- ⁴ Lei, H.; Han, A.; Li, F.; Zhang, M.; Han, Y.; Du, P.; Lai, W.; Cao, R. Electrochemical, Spectroscopic and Theoretical Studies of a Simple Bifunctional Cobalt Corrole Catalyst for Oxygen Evolution and Hydrogen Production. *Phys. Chem. Chem. Phys.* **2014**, *16*, 1883-1893.
- ⁵ Lei, H.; Liu, C.; Wang, Z.; Zhang, Z.; Zhang, M.; Chang, X.; Zhang, W.; Cao, R. Noncovalent Immobilization of a Pyrene-Modified Cobalt Corrole on Carbon Supports for Enhanced Electrocatalytic Oxygen Reduction and Oxygen Evolution in Aqueous Solutions. *ACS Catal.* **2016**, *6*, 6429-6437.

-
- ⁶ Guillard, R.; Gros, C. P.; Bolze, F.; Jérôme, F.; Ou, Z.; Shao, J.; Fischer, J.; Weiss, R.; Kadish, K. M. Alkyl and Aryl Substituted Corroles. 1. Synthesis and Characterization of Free Base and Cobalt Containing Derivatives. X-ray Structure of (Me₄Ph₅Cor)Co(py)₂. *Inorg. Chem.* **2001**, *40*, 4845-4855.
- ⁷ Kadish, K. M.; Shao, J.; Ou, Z.; Gros, C. P.; Bolze, F.; Barbe, J.-M.; Guillard, R. Alkyl- and Aryl-Substituted Corroles. 4. Solvent Effects on the Electrochemical and Spectral Properties of Cobalt Corroles. *Inorg. Chem.* **2003**, *42*, 4062-4070.
- ⁸ Mahammed A.; Giladi I.; Goldberg I.; Gross Z. Synthesis and Structural Characterization of a Novel Covalently-Bound Corrole Dimer. *Chem. Eur. J.* **2001**, *7*, 4259-4265.
- ⁹ Wang, Z.; Lei, H.; Cao, R.; Zhang, M. Cobalt Corrole on Carbon Nanotube as a Synergistic Catalyst for Oxygen Reduction Reaction in Acid Media. *Electrochim. Acta* **2015**, *171*, 81-88.
- ¹⁰ Simkhovich, L.; Goldberg, I.; Gross, Z. Easy Preparation of Cobalt Corrole and Hexaphyrin and Isolation of New Oligopyrroles in the Solvent-Free Condensation of Pyrrole with Pentafluorobenzaldehyde. *Org. Lett.* **2003**, *5*, 1241-1244.
- ¹¹ Huang, S.; Fang, Y.; Lü, A.; Lu, G.; Ou, Z.; Kadish, K. M. Synthesis, Characterization and Solvent/Structural Effects on Spectral and Redox Properties of Cobalt Triphenylcorroles in Nonaqueous Media. *J. Porphyrins Phthalocyanines* **2012**, *16*, 958-967.
- ¹² Koszarna, B.; Gryko, D. T. Efficient Synthesis of *meso*-Substituted Corroles in a H₂O–MeOH Mixture. *J. Org. Chem.* **2006**, *71*, 3707-3717.
- ¹³ Capar, J.; Berg, S.; Thomas, K. E.; Beavers, C. M.; Gagnon, K. J.; Ghosh, A. Improved Syntheses of β -Octabromo-*meso*-Triarylcorrole Derivatives. *J. Inorg. Biochem.* **2015**, *153*, 162-166.
- ¹⁴ Thomas, K. E.; Conradie, J.; Hansen, L. K.; Ghosh, A. Corroles Cannot Ruffle. *Inorg. Chem.* **2011**, *50*, 3247–3251.
- ¹⁵ Pomarico, G.; Tortora, L.; Fronczek, F. R.; Smith, K. M.; Paolesse, R. Selective Nitration and Bromination of Surprisingly Ruffled Phosphorus Corroles. *J. Inorg. Biochem.* **2016**, *158*, 17-23.
- ¹⁶ Gao, D.; Azarias, C.; D'Aléo, A.; Giorgi, M.; Siri, O.; Balaban, T. S.; Jacquemin, D.; Canard, G. Synthesis and Characterization of Ruffled Phosphorus *meso*-Ester Corroles. *Eur. J. Inorg. Chem.* **2017**, *2017*, 780-788.

-
- ¹⁷ Maiti, N.; Lee, J.; Kwon, S. J.; Kwak, J.; Do, Y.; Churchill, D. G. Synthetic, Crystallographic and Electrochemical Studies of Thienyl-substituted Corrole Complexes of Copper and Cobalt. *Polyhedron* **2006**, *25*, 1519-1530.
- ¹⁸ Ooi, S.; Tanaka, T.; Osuka, A. Cobalt(III) and Gallium(III) Complexes of *meso*-Free Corroles with Distinct Position-Dependent Substituent Effects. *J. Porphyrins Phthalocyanines* **2016**, *20*, 274-281.
- ¹⁹ Ooi, S.; Tanaka, T.; Osuka, A. Metal Complexes of *meso*-*meso* Linked Corrole Dimers. *Inorg. Chem.* **2016**, *55*, 8920-8927.
- ²⁰ Saltsman, I.; Goldberg, I.; Gross, Z. Porphyrins and Corroles with 2,6-Pyrimidyl Substituents. *Org. Lett.* **2015**, *17*, 3214-3217.
- ²¹ Mahammed, A.; Botoshansky, M.; Gross, Z. Chlorinated corroles. *Dalton Trans.* **2012**, *41*, 10938-10940.
- ²² The Co-complex after preparative TLC purification is dissolved in DCM to which 3-4 drops of pyridine is added. The brown DCM solution turns intense green in presence of pyridine. The solution is evaporated on rotary evaporator under high vacuum, the residue re-dissolved in 1:1 DCM/ hexane and evaporated again at high temperature under high vacuum. The residue was finally kept under a strong stream of nitrogen gas for some time to ensure complete evaporation of all residual solvent vapours. Finally the green residue is taken into CDCl₃ to make a fairly concentrated solution (~ 0.005 g in ~ 1 mL solvent). The NMR spectrum recorded afterwards shows no sign of residual DCM or pyridine solvents.
- ²³ Ghosh, A. Electronic Structure of Corrole Derivatives: Insights from Molecular Structures, Spectroscopy, Electrochemistry, and Quantum Chemical Calculations. *Chem. Rev.* **2017**, *117*, 3798-3881.
- ²⁴ Johansen, I.; Norheim, H.-K.; Larsen, S.; Alemayehu, A. B.; Conradie, J.; Ghosh, A. Substituent Effects on Metalloporrole Spectra: Insights from Chromium-Oxo and Molybdenum-Oxo Triarylcorroles. *J. Porphyrins Phthalocyanines* **2011**, *15*, 1335-1344.
- ²⁵ Einrem, R. F.; Braband, H.; Fox, T.; Vazquez-Lima, H.; Alberto, R.; Ghosh, A. Synthesis and molecular structure of ⁹⁹Tc Corroles. *Chem. Eur. J.* **2016**, *22*, 18747-18751.
- ²⁶ Einrem, R. F.; Gagnon, K. J.; Alemayehu, A. B.; Ghosh, A. Metal-Ligand Misfits: Facile Access to Rhenium-Oxo Corroles by Oxidative Metalation. *Chem. Eur. J.* **2016**, *22*, 517-520.

- ²⁷ Alemayehu, A. B.; Vazquez-Lima, H. Gagnon, K. J.; Ghosh, A. Stepwise Deoxygenation of Nitrite as a Route to Two Families of Ruthenium Corroles: Group 8 Periodic Trends and Relativistic Effects. *Inorg. Chem.* **2017**, *56*, 5285–5294.
- ²⁸ Alemayehu, A. B.; Gagnon, K. J.; Turner, J.; Ghosh, A. Oxidative Metalation as a Route to Size-Mismatched Macrocyclic Complexes: Osmium Corroles. *Angew. Chem. Int. Ed.* **2014**, *53*, 14411-14414.
- ²⁹ Alemayehu, A. B.; Ghosh, A. Gold Corroles. *J. Porphyrins Phthalocyanines* **2011**, *15*, 106-110.
- ³⁰ Rabinovitch, E.; Goldberg, I.; Gross, Z. Gold(I) and Gold(III) Corroles. *Chem. Eur. J.* **2011**, *17*, 12294–12301.
- ³¹ Thomas, K. E.; Alemayehu, A. B.; Conradie, J.; Beavers, C.; Ghosh, A. Synthesis and Molecular Structure of Gold Triarylcorroles. *Inorg. Chem.* **2011**, *50*, 12844–12851.
- ³² Steene, E.; Wondimagegn, T.; Ghosh, A. Electrochemical and Electronic Absorption Spectroscopic Studies of Substituent Effects in Iron(IV) and Manganese(IV) Corroles. Do the Compounds Feature High-Valent Metal Centers or Noninnocent Corrole Ligands? Implications for Peroxidase Compound I and II Intermediates. *J. Phys. Chem. B* **2001**, *105*, 11406-11413. Addition/correction: *J. Phys. Chem. B* **2002**, *106*, 5312-5312.
- ³³ Zakhariyeva, O.; Schünemann, V.; Gerdan, M.; Licocchia, S.; Cai, S.; Walker, F. A.; Trautwein, A. X. Is the Corrolate Macrocycle Innocent or Noninnocent? Magnetic Susceptibility, Mössbauer, ¹H NMR, and DFT Investigations of Chloro- and Phenyliron Corrolates. *J. Am. Chem. Soc.* **2002**, *124*, 6636-6648.
- ³⁴ Walker, F. A.; Licocchia, S.; Paolesse, R. Iron Corrolates: Unambiguous Chloroiron(III) (Corrolate)²⁻ π -Cation Radicals. *J. Inorg. Biochem.* **2006**, *100*, 810-837.
- ³⁵ Vazquez-Lima, H.; Norheim, H. K.; Einrem, R. F.; Ghosh, A. Cryptic Noninnocence: FeNO Corroles in a New Light. *Dalton Trans.* **2015**, *44*, 10146-10151.
- ³⁶ Norheim, H.-K.; Capar, J.; Einrem, R. F.; Gagnon, K. J.; Beavers, C. M.; Vazquez-Lima, H.; Ghosh, A. Ligand Noninnocence in FeNO Corroles: Insights from β -Octabromocorrole Complexes. *Dalton Trans.* **2016**, *45*, 681-689.
- ³⁷ Ganguly, S.; Vazquez-Lima, H.; Ghosh, A. Wolves in Sheep's Clothing: μ -Oxo-Diiron Corroles Revisited. *Chem. Eur. J.* **2016**, *22*, 10336-10340.

- ³⁸ Wasbotten, I. H.; Wondimagegn, T.; Ghosh, A. Electronic Absorption, Resonance Raman, and Electrochemical Studies of Planar and Saddled Copper(III) *Meso*-Triarylcorroles. Highly Substituent-Sensitive Soret Bands as a Distinctive Feature of High-Valent Transition Metal Corroles. *J. Am. Chem. Soc.* **2002**, *124*, 8104-8116.
- ³⁹ Steene, E.; Dey, A.; Ghosh, A. β -Octafluorocorroles. *J. Am. Chem. Soc.* **2003**, *125*, 16300-16309.
- ⁴⁰ Brückner, C.; Briñas, R. P.; Bauer, J. A. K. X-ray Structure and Variable Temperature NMR Spectra of [*meso*-Triarylcorrolato]copper(III). *Inorg. Chem.* **2003**, *42*, 4495–4497.
- ⁴¹ Bröring, M.; Bregier, F.; Tejero E. C.; Hell, C.; Holthausen M. C. Revisiting the Electronic Ground State of Copper Corroles. *Angew. Chem., Int. Ed.* **2007**, *46*, 445–448.
- ⁴² Thomas, K. E.; Wasbotten, I. H.; Ghosh, A. Copper β -Octakis(Trifluoromethyl)Corroles: New Paradigms for Ligand Substituent Effects in Transition Metal Complexes. *Inorg. Chem.* **2008**, *47*, 10469-10478.
- ⁴³ Alemayehu, A. B.; Hansen, L. K.; Ghosh, A. Nonplanar, Noninnocent, and Chiral: A Strongly Saddled Metalloporrole. *Inorg. Chem.* **2010**, *49*, 7608-7610.
- ⁴⁴ Thomas, K. E.; Conradie, J.; Hansen, L. K.; Ghosh, A. A Metalloporrole with Orthogonal Pyrrole Rings. *Eur. J. Inorg. Chem.* **2011**, 1865–1870.
- ⁴⁵ Berg, S.; Thomas, K. E.; Beavers, C. M.; Ghosh, A. Undecaphenylcorroles. *Inorg. Chem.* **2012**, *51*, 9911-9916.
- ⁴⁶ Thomas, K. E.; Vazquez-Lima, H.; Fang, Y.; Song, Y.; Gagnon, K. J.; Beavers, C. M.; Kadish, K. M.; Ghosh, A. Ligand Noninnocence in Coinage Metal Corroles: A Silver Knife-Edge. *Chem. - Eur. J.* **2015**, *21*, 16839-16847.
- ⁴⁷ Alemayehu, A. B.; Vazquez-Lima, H.; Beavers, C. M.; Gagnon, K. J.; Bendix, J.; Ghosh, A. Platinum Corroles. *Chem. Comm.* **2014**, *50*, 11093-11096.
- ⁴⁸ Alemayehu, A.; Conradie, J.; Ghosh, A. A First TDDFT Study of Metalloporrole Electronic Spectra: Copper *meso*-Triarylcorroles Exhibit Hyper Spectra. *Eur. J. Inorg. Chem.* **2011**, *2011*, 1857-1864.
- ⁴⁹ Ghosh, A.; Wondimagegn, T.; Parusel, A. B. J. Electronic Structure of Gallium, Copper, and Nickel Complexes of Corrole. High-Valent Transition Metal Centers Versus Noninnocent Ligands. *J. Am. Chem. Soc.* **2000**, *122*, 5100-5104.
- ⁵⁰ Ghosh, A.; Steene, E. High-Valent Transition Metal Centers and Noninnocent Ligands in

Metalloporphyrins and Related Molecules: A Broad Overview Based on Quantum Chemical Calculations. *J. Biol. Inorg. Chem.* **2001**, *6*, 739-752.

⁵¹ Fang, Y.; Ou, Z.; Kadish, K. M. Electrochemistry of Corroles in Nonaqueous Media. *Chem. Rev.* **2017**, *117*, 3377-3419.

⁵² Capar, C.; Thomas, K. E.; Ghosh, A. Reductive Demetalation of Copper Corroles: First Simple Route to Free-Base β -octabromocorroles. *J. Porphyrins Phthalocyanines* **2008**, *12*, 964–967.

⁵³ Orłowski, R.; Gryko, D. T. Synthesis of Corroles and Their Heteroanalogs. *Chem. Rev.* **2017**, *117*, 3102–3137.

⁵⁴. Sheldrick, G. M. SHELXT - Integrated Space-Group and Crystal-Structure Determination. *Acta Cryst.* **2015**, *A71*, 3-8.

⁵⁵. Sheldrick, G. M. Crystal Structure Refinement with SHELXL. *Acta Cryst.* **2015**, *C71*, 3-8.

⁵⁶ Becke, A.D.; Density-Functional Exchange-Energy Approximation with Correct Asymptotic Behaviour. *Phys. Rev. A*, **1988**, *38*, 3098-3100.

⁵⁷ Lee, C.T.; Yang, W.T.; Parr, R.G. Development of the Colle-Salvetti Correlation-Energy Formula into a Functional of the Electron-Density. *Phys. Rev. B*, **1988**, *37*, 785-789.

⁵⁸. Grimme, S.; Anthony, J.; Ehrlich, S.; Krieg, H. A Consistent and Accurate *Ab Initio* Parametrization of Density Functional Dispersion Correction (DFT-D) for the 94 Elements H-Pu. *J. Chem. Phys.* **2010**, *132*, Art. no. 154104.

⁵⁹ Velde, G. T.; Bickelhaupt, F. M.; Baerends, E. J.; Guerra, C. F.; van Gisbergen, S. J. A.; Snijders, J. G.; Ziegler, T. Chemistry with ADF. *J. Comput. Chem.* **2001**, *22*, 931-967.

Table of content entry:

UV-vis spectroscopy and broken-symmetry DFT (B3LYP-D3) calculations indicate an antiferromagnetically coupled Co^{II} -corrole²⁻ formulation for five-coordinate cobalt-corrole-pyridine intermediates.

